Review of Plots from ATHENA/ECCE(/CORE)

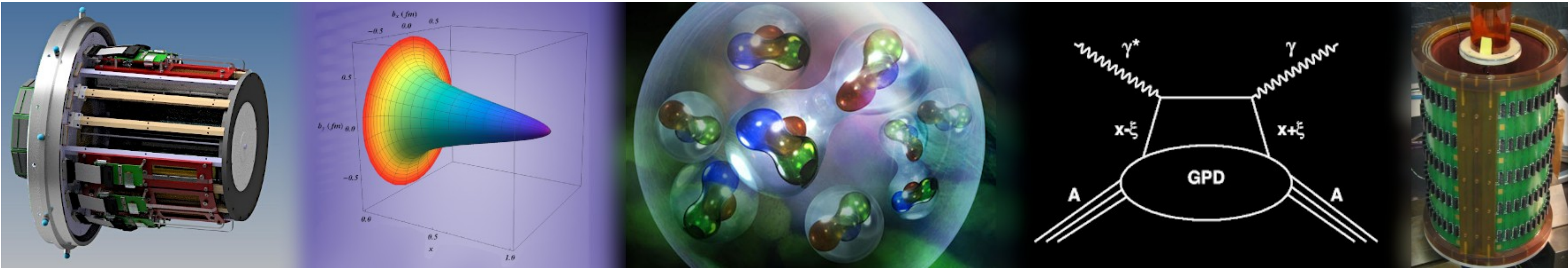

Raphaël Dupré
&
Rachel Montgomery

Introduction

This talk sounded like a good idea

- Then we realized there are a lot of figures to cover
  - **And it is very different from one channel to another**
- So, I will only make very general comments
  - **The talk can also serve as reference, but with many limitations as we will see**

Still there is a reason behind it

- We want to constitute a base for talks about EDT physics
  - **Exclusive, diffractive and tagging measurements**
- A new set of ePIC figure to replace ECCE/Athena
- Prepare the TDR and the associated physics paper
  - **We need to illustrate how the ePIC design makes possible the physics**

Request from the collaboration

Types of Figures

- New figures that can be labeled ePIC
- Old figures we really would like to reproduce
- Old figures that are not as important

Information

- Title and author and and an integrated ePIC logo
- Dataset, luminosity assumed, and software version used to produce the figure
- Few lines of explanation and link to AoS goals for EIC

Goals of this Session

We have very different take between ECCE/Athena

- The type and numbers of figures in the proposals and other documents vary wildely
- We should reflect on this and think about what we want for ePIC

This is a working session !

- The talk presents our first findings
- But we are likely missing a lot

So please participate !

- Interrupt and let us know your opinion
- We will take notes and will make a summary

ECCE - DVCS ep

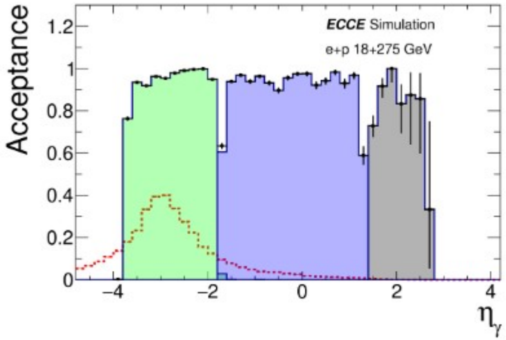

Figure 31: DVCS photon acceptance in the backward (green), barrel (blue), and forward (grey) ECAL's, as a function of pseudorapidity. The red dotted line shows the distribution of (generated) DVCS photons

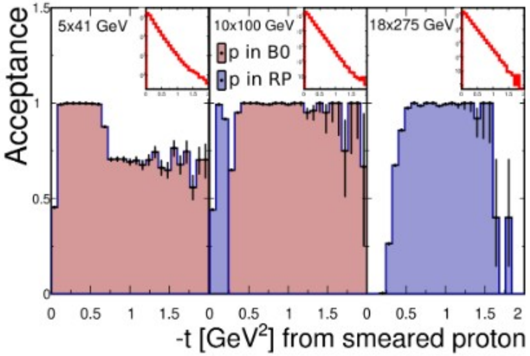

Figure 32: Acceptance for DVCS protons as a function of $-t$ in the far-forward detectors for different beam energy configurations. The inserts show the $-t$ distributions of generated events.

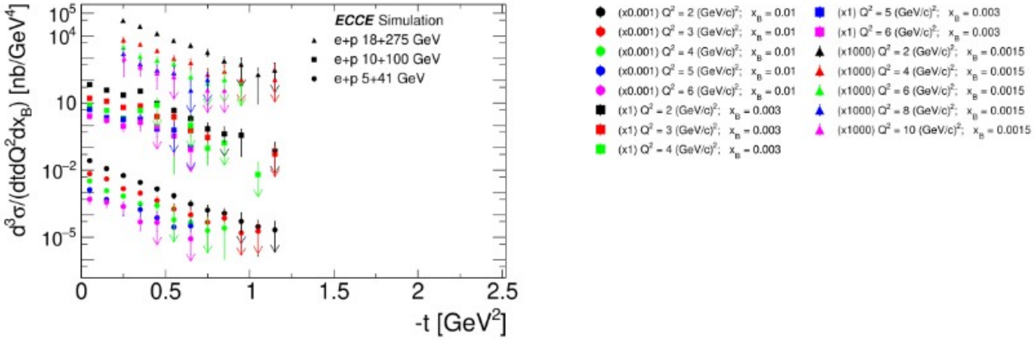

Figure 33: Projected DVCS differential cross-section measurements as a function of the momentum transfer $-t$ for different bins in Q^2 and x_B. The assumed integrated luminosity is 10 fb $^{-1}$ for each beam energy configuration.

Figures in ATHENA/ECCE proposals

Kinematic coverage

- Standard values (Q2, x, t…)

Detector oriented

- In which detector do the particles go, what coverage do we have
-
-
-
-
-

The results plots

- Observable projections
-

ATHENA DVCS

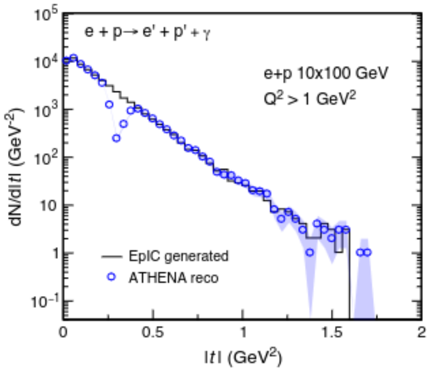

Figure 36. The $|t|$ distribution of DVCS events in e+p collisions from the EpIC Monte Carlo Generator (black line) for 10 GeV electron and 100 GeV proton beam energies, is compared with the reconstructed distribution (blue circles) (FullSim).

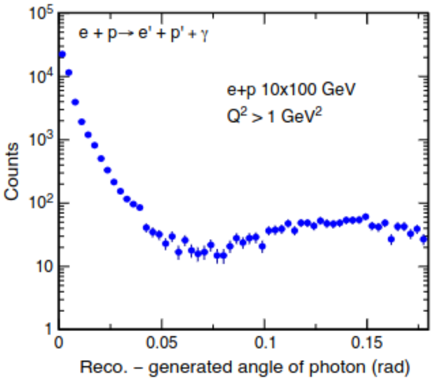

Figure 37. Difference between the generated and reconstructed angle of the produced real photon in a DVCS event simulated in e+p collisions for the 10 GeV electron and 100 GeV proton beam energies (FullSim).

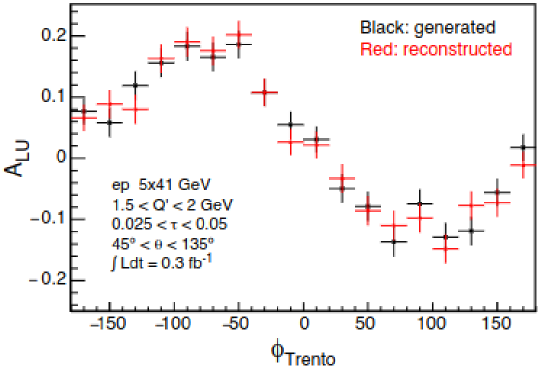

Figure 38. Beam-spin asymmetry A_{LU} extracted from generated (black squares) and reconstructed (red circles) data as a function of ϕ_{Trento} in polarized e+p collisions of 5 GeV electrons and 41 GeV protons with statistical uncertainties corresponding to ~ 0.3 fb^{-1}. The data show the kinematic bin of $1.5 < Q' < 2$ GeV, $0.025 < \tau < 0.05$ and $45^o < \theta < 135^o$, where Q' is the invariant mass of the lepton pair, which provides the hard scale in the process, $\tau = Q'^2/(s - m_p^2)$ is the equivalent of x for TCS and θ is the angle between a produced lepton and the scattered proton (FullSim).

Figures in ATHENA/ECCE proposals

Kinematic coverage

- Standard values (Q2, x, t…)

Detector oriented

- In which detector do the particles go, what coverage do we have
-
- Resolution figure to isolate this specific channel
-
-
-

The results plots

- Observable projections
-

ECCE - DVCS eA

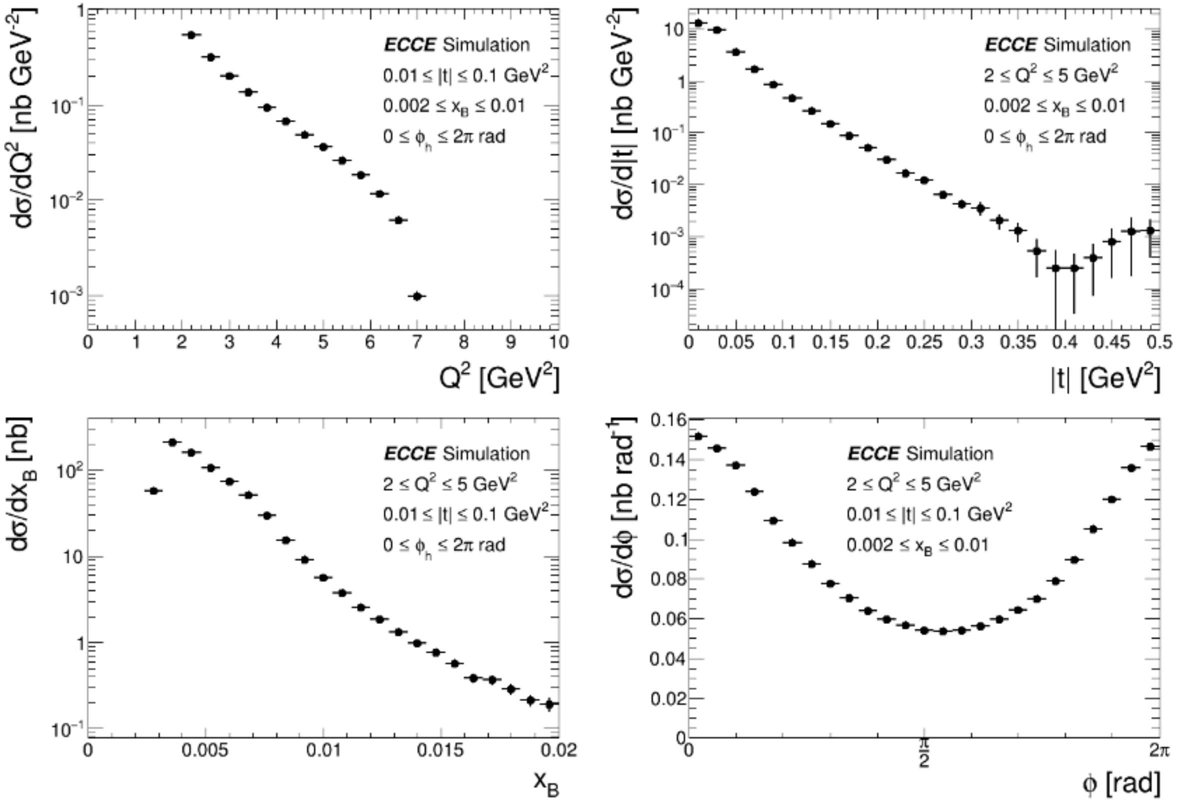

Figure 35: Projected differential cross-sections in ECCE as functions of physics variables Q^2, x_B, $-t$ and ϕ for DVCS-e^{4}He. Each plot is integrated over the phase space denoted in the legend.

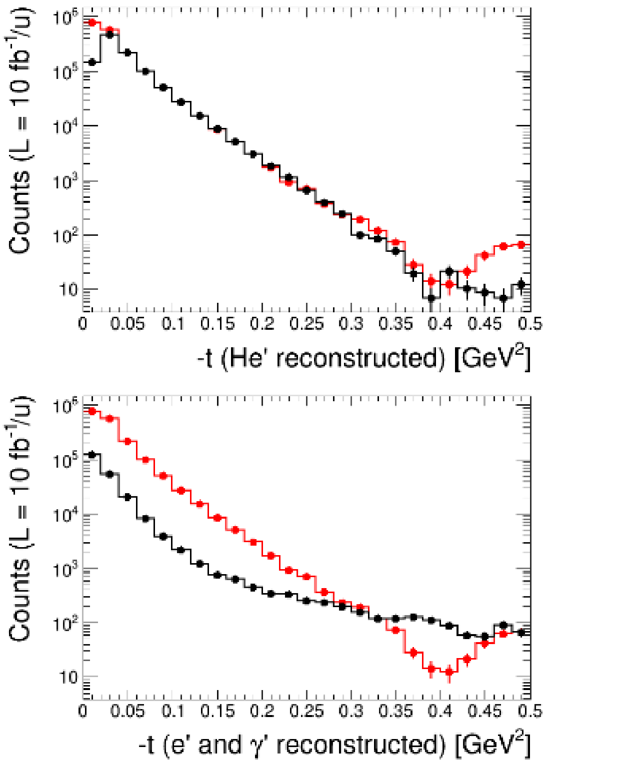

Figure 34: Reconstructed (black) and generated (red) for $-t$ distributions for ($e\,^4$He, $e'\,^4$He$'\,\gamma$), using different methods, as described in the body of text, and normalized to the EIC luminosity.

Figures in ATHENA/ECCE proposals

Kinematic coverage

- Either standard (Q2, x, t…) or channel specific

Detector oriented

- In which detector do the particles go, what coverage do we have
-
- Resolution figure to isolate this specific channel

Analysis exploration

-
-
- Different analysis techniques (or detector technologies)

The results plots

- Observable projections
-

ATHENA DVMP Phi

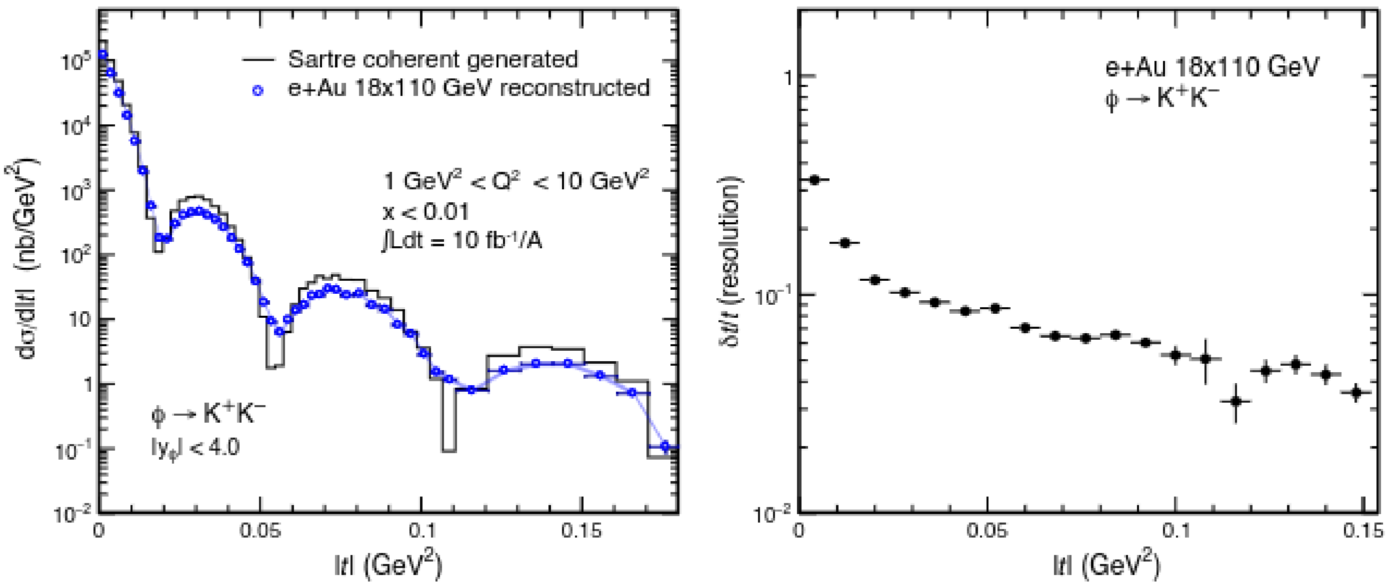

Figure 45. Left: differential $|t|$ distribution of diffractive ϕ-mesons in e+Au collisions of 18 GeV electron beams with 110 GeV Au beams. Distributions of the coherent differential cross section from the Sartre event generator and its reconstruction with ATHENA ("Method L") are shown. Right: the corresponding $|t|$ resolutions versus the generated $|t|$ (FastSim).

Figures in ATHENA/ECCE proposals

Kinematic coverage

- Either standard (Q2, x, t…) or channel specific

Detector oriented

- In which detector do the particles go, what coverage do we have
-
- Resolution figure to isolate this specific channel

Analysis exploration

- Observable resolution
-
- Different analysis techniques (or detector technologies)

The results plots

- Observable projections
-

ATHENA DVMP J/Psi

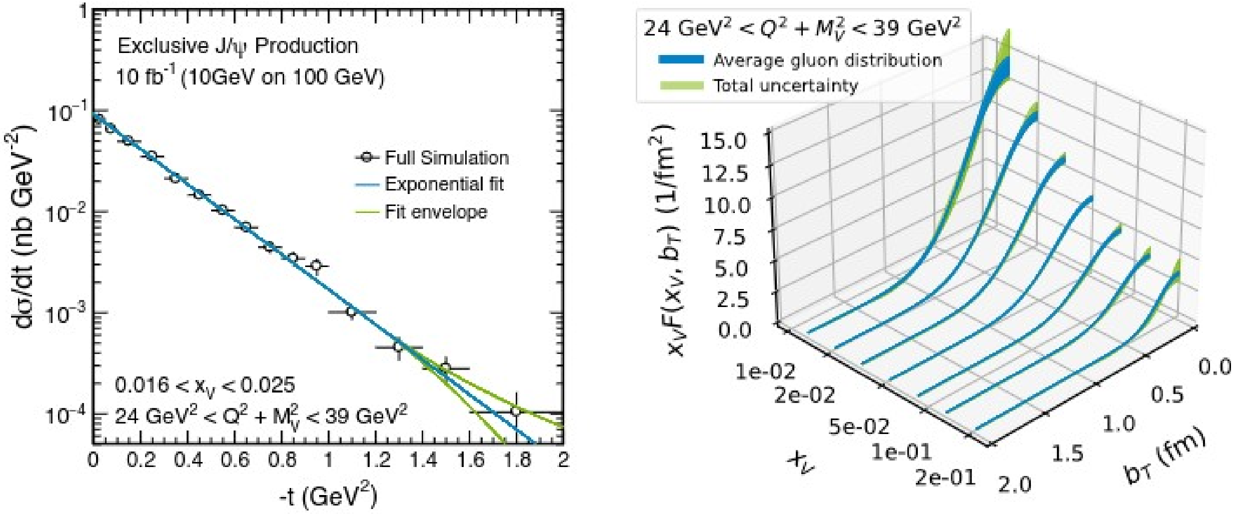

Figure 39. Left: exclusive J/ψ differential production cross section in the e^+e^- decay channel for $0.016 < x_V < 0.025$ and $24\,\text{GeV}^2 < Q^2 + M_V^2 < 39\,\text{GeV}^2$. The blue central curve is an exponential fit to the pseudodata, while the green outer curves show the extremes of various extrapolation scenarios outside of the measured range (FullSim). Right: the corresponding b_T and x_V dependence of the extracted gluon transverse profiles, multiplied with the gluon PDF from CT14 [109], for the same bin in $Q^2 + M_V^2$. The blue band shows the statistical uncertainty, while the green band shows the total uncertainty, including the extrapolation uncertainty of the Fourier transform (FullSim).

Figures in ATHENA/ECCE proposals

Kinematic coverage

- Either standard (Q2, x, t…) or channel specific

Detector oriented

- In which detector do the particles go, what coverage do we have
-
- Resolution figure to isolate this specific channel

Analysis exploration

- Observable resolution
-
- Different analysis techniques (or detector technologies)

The results plots

- Observable projections
- Global fit projections and phenomenology applied on pseudo data

ECCE - DVMP J/Psi

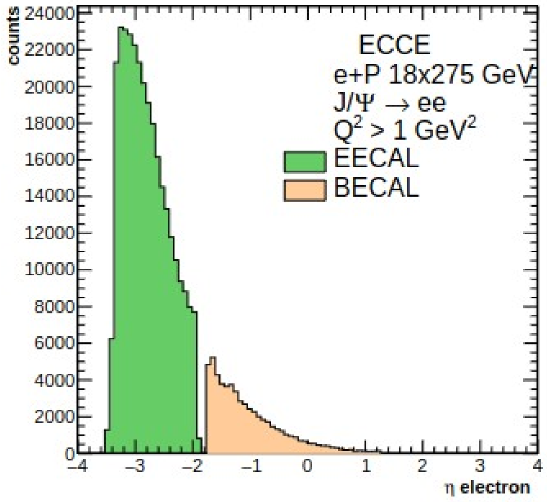

Figure 36: Scattered electron detection in the calorimeters. Most of the electrons go to the far backward region.

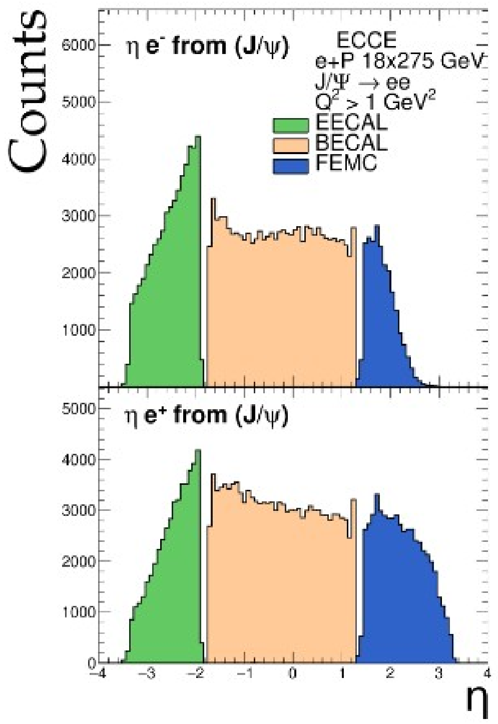

Figure 37: Electron (left) and positron (right) from J/ψ detection in the calorimeters.

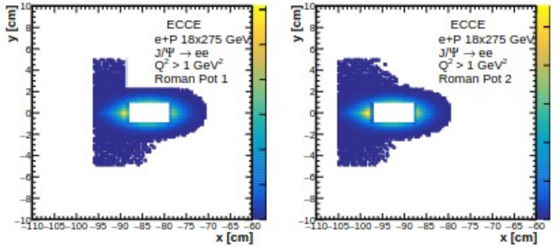

Figure 38: Proton detection in Roman Pot 1 (left) and Roman Pot 2 (right) for the kinematic setting studied in this work.

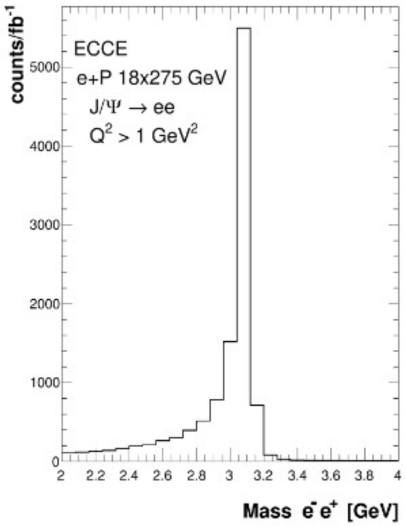

Figure 39: Reconstructed J/ψ mass, for the 18x275 GeV kinematic setting.

ECCE - DVMP J/Psi

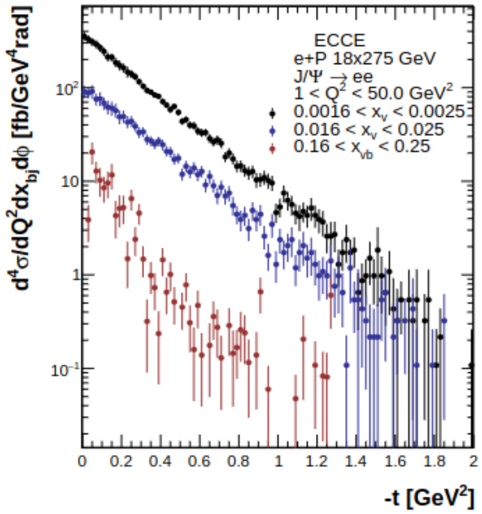

Figure 41: Differential cross-section vs Momentum transfer t for the 18×275 beam setting studied in x_v slices, $0.0016 < x_v < 0.0025$ (black), $0.016 < x_v < 0.025$ (blue) and $0.16 < x_v < 0.25$ (red).

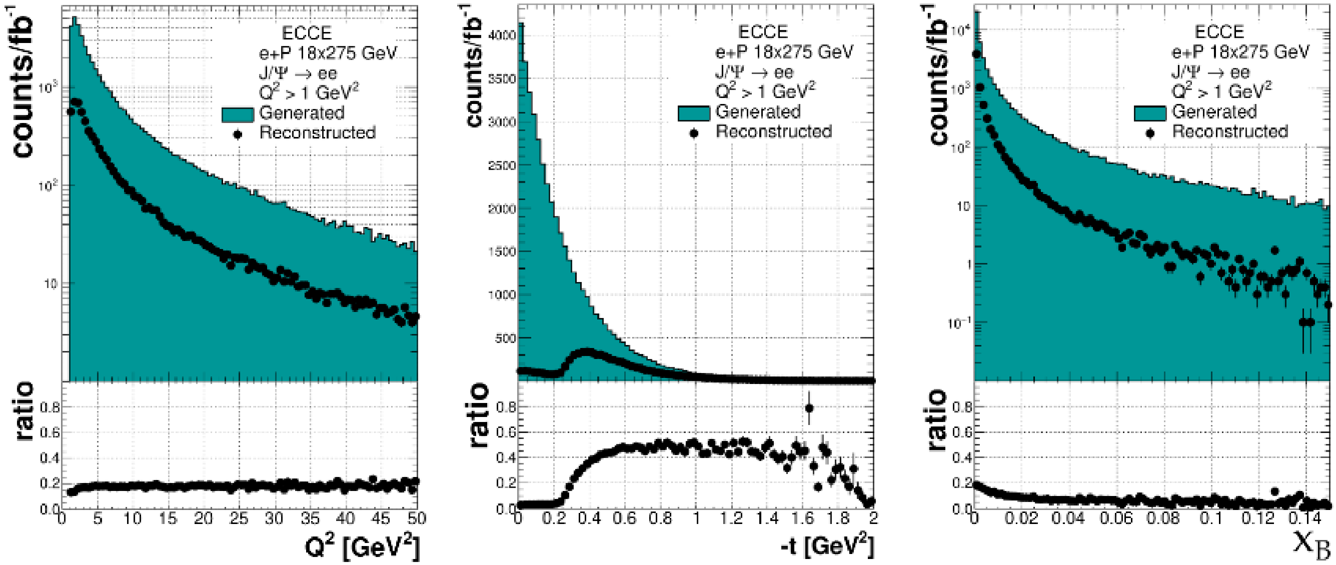

Figure 40: Physics kinematicas variables and resolutions for ep scattering of 18x275 GeV^2.

Figures in ATHENA/ECCE proposals

Kinematic coverage

- Either standard (Q2, x, t…) or channel specific

Detector oriented

- In which detector do the particles go, what coverage do we have
- Acceptance/efficiency of the detector setup
- Resolution figure to isolate this specific channel

Analysis exploration

- Observable resolution
-
- Different analysis techniques (or detector technologies)

The results plots

- Observable projections
- Global fit projections and phenomenology applied on pseudo data

ECCE - TCS

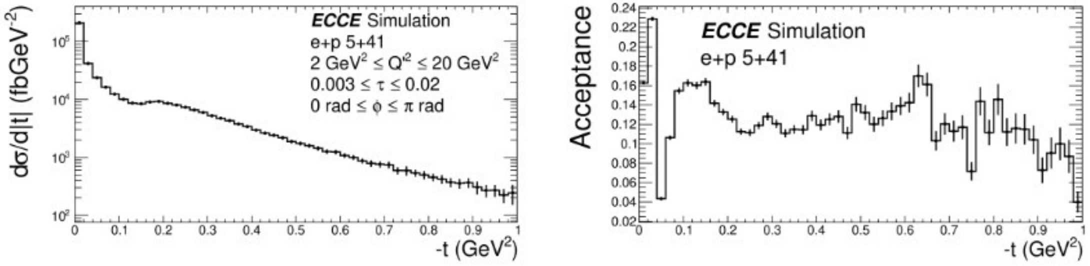

Figure 43: 5×41 - TCS Differential cross-section versus the momentum transfer to the struck parton $-t$ reconstructed using the beam and scattered protons $t = (p - p')^2$ (left) and detector acceptance for $-t$ reconstructed using the beam and scattered protons (right). Note acceptance is given as a value where 1 corresponds to 100%

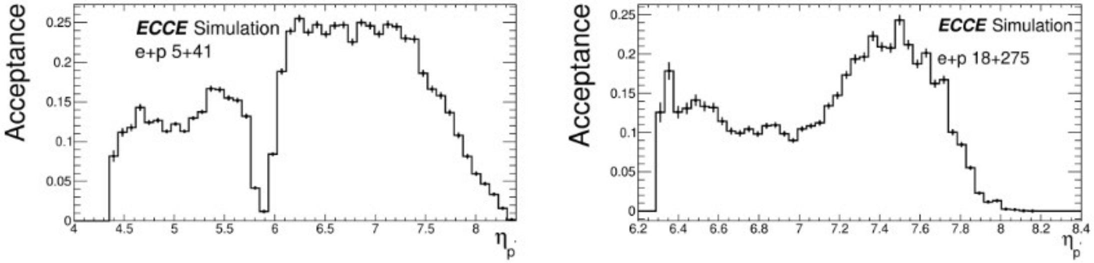

Figure 44: Left: 5×41 acceptance vs pseudorapidity (η) of the scattered proton from TCS events. Right: 18×275 acceptance vs pseudorapidity (η) of the scattered proton. Note acceptance is given as a value where 1 corresponds to 100%

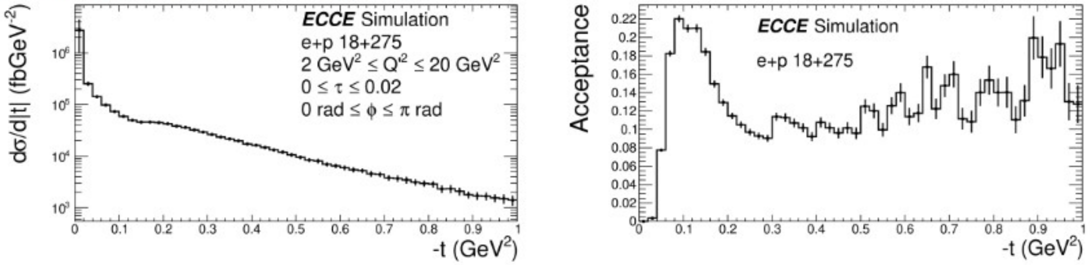

Figure 45: 18×275 - TCS Differential cross-section versus the momentum transfer to the struck parton $-t$ (left) and detector acceptance for $-t$ (right). Note acceptance is given as a value where 1 corresponds to 100%

ATHENA Upsilon

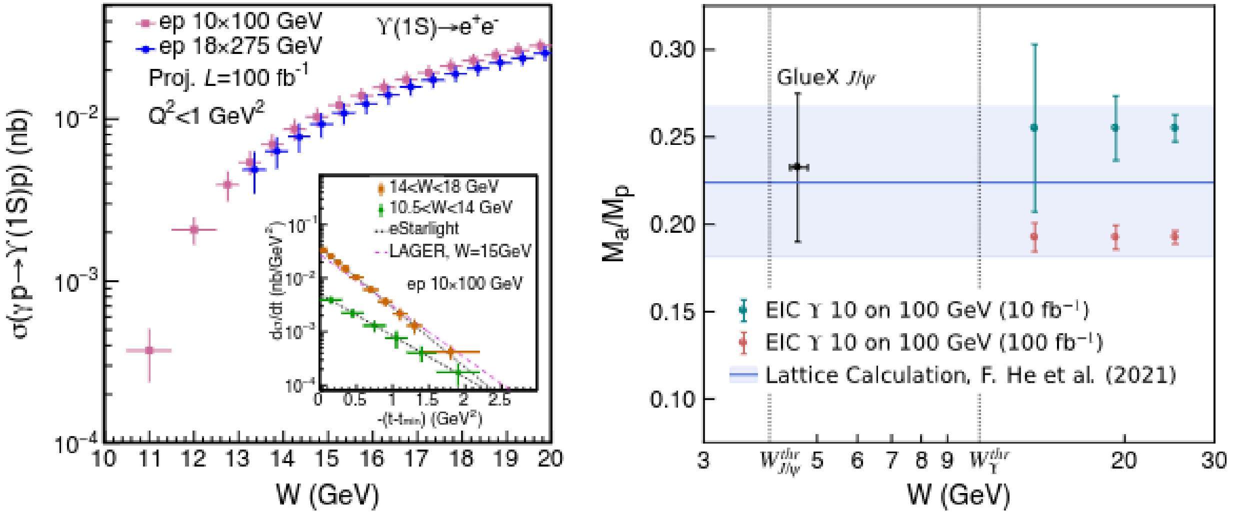

Figure 40. Left: the projected uncertainty of the total and differential (insertion) cross sections of $\Upsilon(1S)$ near-threshold for photoproduction and electroproduction ($Q^2 < 1\,\mathrm{GeV}^2$) in e+p collisions via the e^+e^- decay channel. Two model predictions [64, 107] of the near threshold differential $d\sigma/dt$ are also shown (FullSim). Right: the trace anomaly contribution to the proton mass in Ji's decomposition according to [110, 111] and references therein. Green and red points correspond to $10\,\mathrm{fb}^{-1}$ and $100\,\mathrm{fb}^{-1}$ integrated luminosity, respectively, and are offset from each other. The band is the result of a recent lattice QCD calculation [112] (FullSim).

Figures in ATHENA/ECCE proposals

Kinematic coverage

- Either standard (Q2, x, t…) or channel specific

Detector oriented

- In which detector do the particles go, what coverage do we have
- Acceptance/efficiency of the detector setup
- Resolution figure to isolate this specific channel

Analysis exploration

- Observable resolution
-
- Different analysis techniques (or detector technologies)

The results plots

- Observable projections sometimes compared to existing data
- Global fit projections and phenomenology applied on pseudo data

ECCE - XYZ Spectroscopy

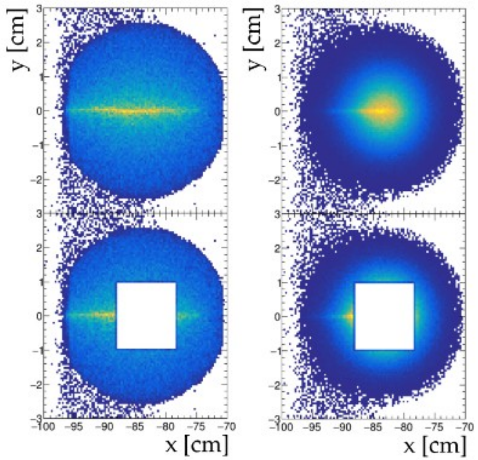

Figure 46: Hit distributions on the first Roman Pot layer for beam settings, left-to-right 5×100 and 18×275. The top row plots show full event distribution; the bottom row plots show the RP acceptance cut applied to remove possible beam backgrounds/contributions.

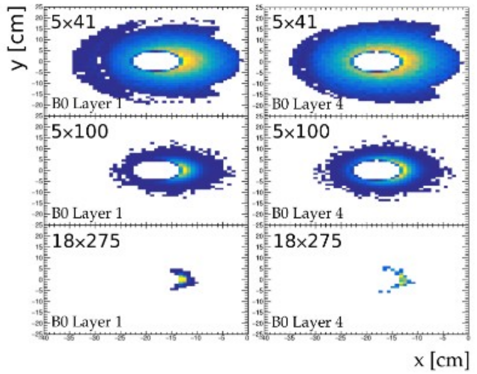

Figure 47: Hit distributions on the four B0 layers for beam settings, top-to-bottom 5×100 and 18×275; with left-to-right front-to-back.

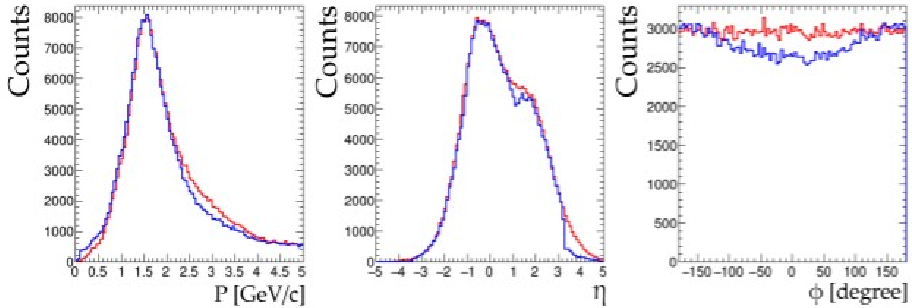

Figure 48: 5×100 generated (red) and reconstructed (blue) J/ψ decay e^- distributions of momentum (P), pseudorapidity (η), and angles (ϕ).

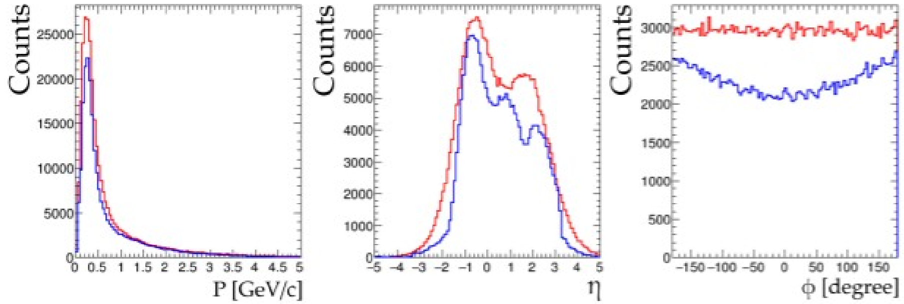

Figure 49: 5×100 generated (red) and reconstructed (blue) π^+ distributions of momentum (P), pseudorapidity (η), and angles (ϕ).

ECCE - XYZ Spectroscopy

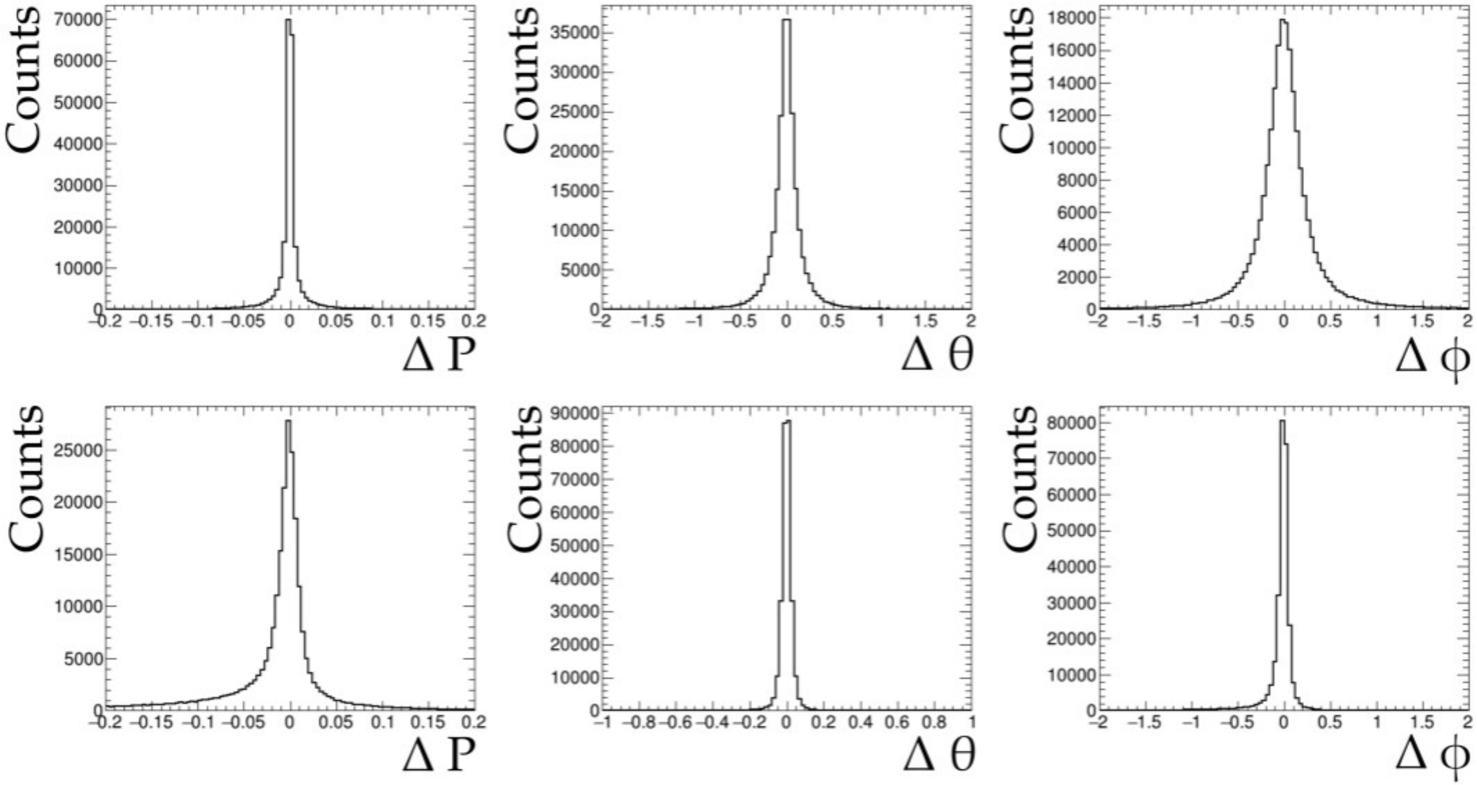

Figure 50: 5x100 π^+ (Top) and e^- (Bottom), resolutions, ΔP, $\Delta\theta$ and $\Delta\phi$ (°), calculated as the difference between reconstructed and truth values.

ECCE - XYZ Spectroscopy

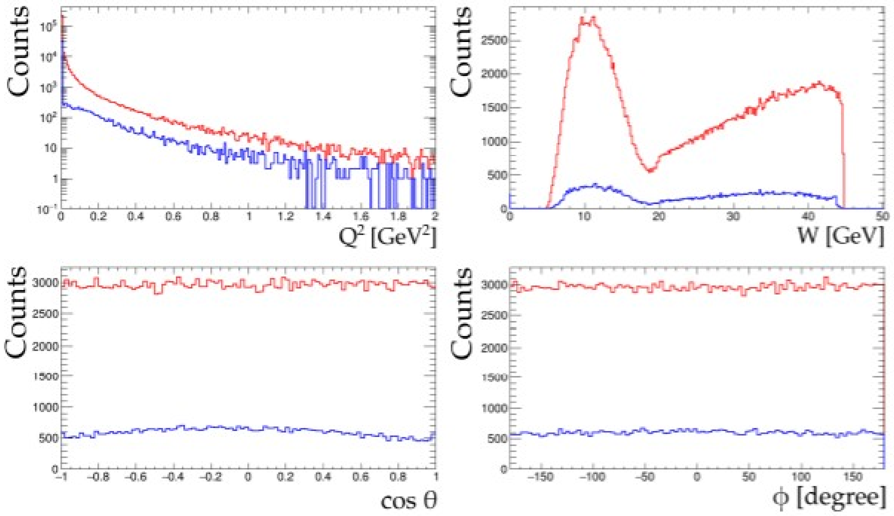

Figure 51: Top: 5x100 generated (red) and reconstructed (blue) distributions of Q^2 and W, for events where all particles were detected. Bottom: 5×100 generated (red) and reconstructed (blue) distributions of the produced meson decay angles in the Gottfried-Jackson reference frame, $\cos\theta$ and ϕ (°), for events where all particles were detected.

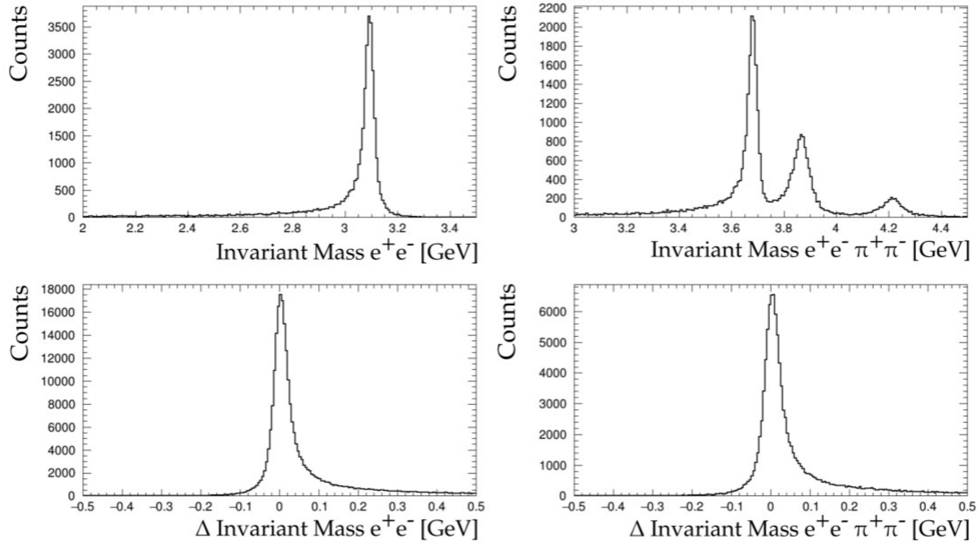

Figure 52: Top: reconstructed invariant masses for meson decay products, the three states of interest are clearly observed on the right plot. Bottom: shows the difference in reconstructed to truth masses.

ECCE - neutron spin PDF via tagging on He3

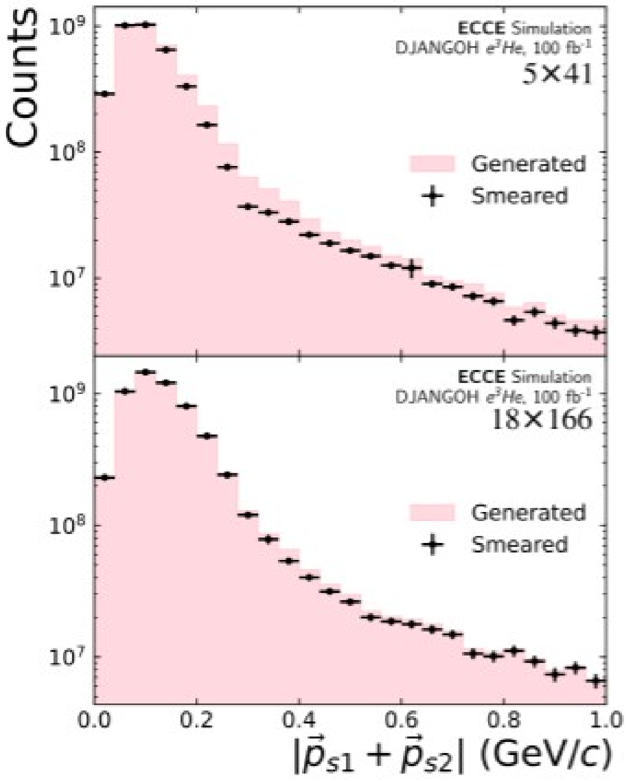

Figure 25: Distribution of the momentum vector sum of two spectator protons, $\vec{p}_{s1}$ and $\vec{p}_{s2}$, in the ion rest frame, for 5×41 (top) and 18×166 (bottom).

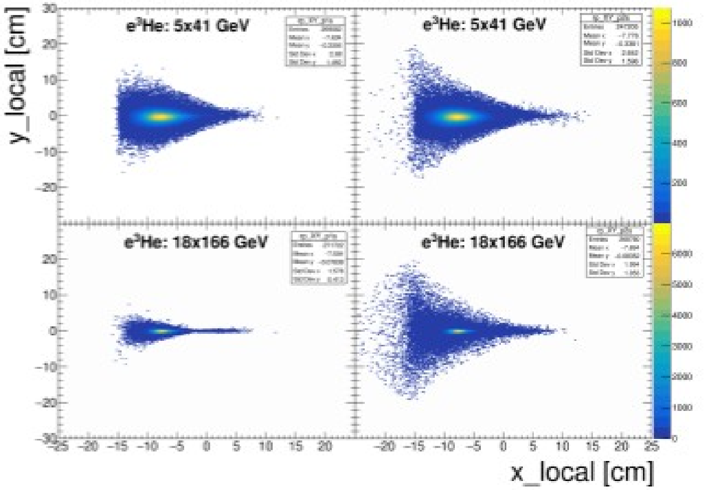

Figure 26: The Roman Pot occupancy layer 1 for spectator proton 1 (left) and spectator proton 2 (right) for the double tagging events

ECCE - neutron spin PDF via tagging on He3

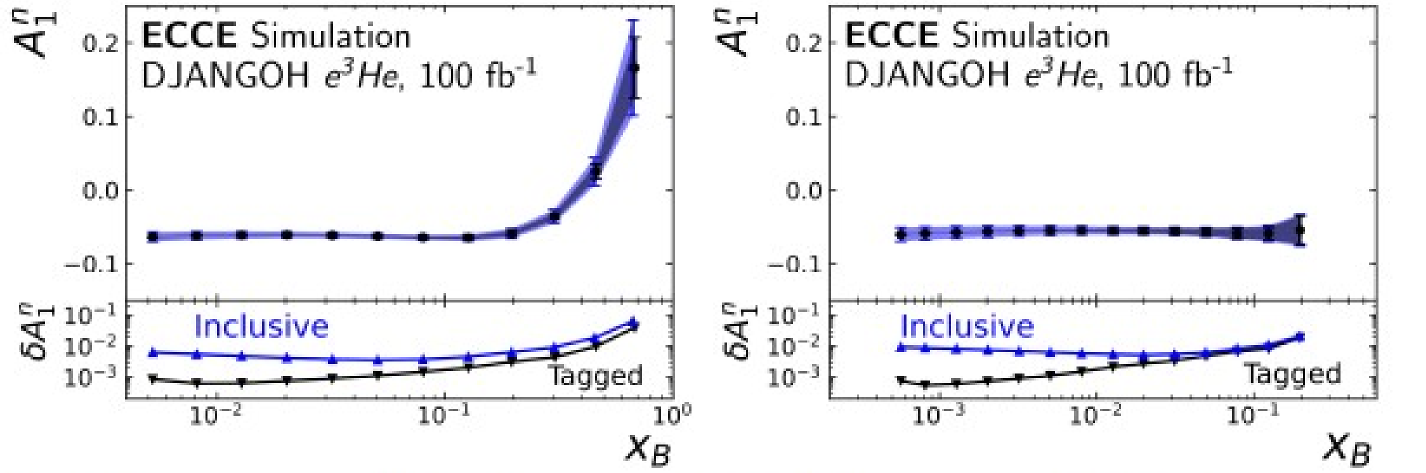

Figure 27: A direct comparison of extracted A_1^n from inclusive measurements (blue band) and double tagging measurements (black square) which are superimposed on the blue band. The left plot is for beam energy setting 5×41 and the right plot is for 18×166. The blue points are the $A_1^{^3\mathrm{He}}$ measured values from inclusive measurements from which the blue band is extracted. The uncertainties for both techniques are compared in the bottom box where the blue (black inverted) triangles are the absolute uncertainties of inclusive (tagged) measurements. The data points were located at the average value for each x_B bin. The asymmetry calculation for each data point corresponds to the average value of Q^2 for each x_B bin.

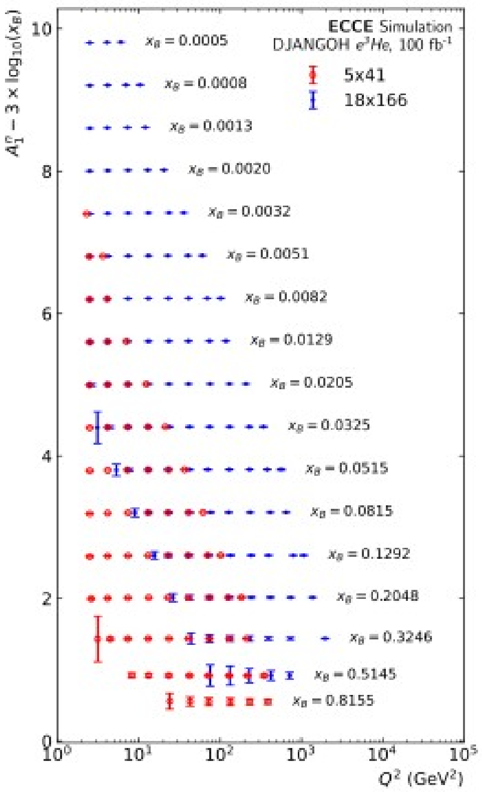

Figure 28: The EIC kinematic coverage of the neutron asymmetry A_1^n as a functions of x_B and Q^2 for two electron-nucleon energy settings 5×41 and 18×166.

ECCE - pion structure function

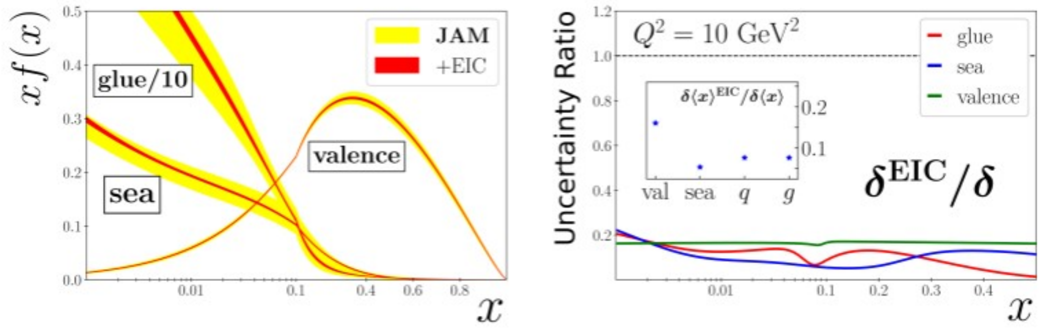

Figure 22: *Left:* Comparison of uncertainties on the pion's valence, sea quark, and gluon PDFs before (yellow bands) and after (red bands) inclusion of EIC data. *Right:* Ratio of uncertainties with EIC data to without, $\delta^{\mathrm{EIC}}/\delta$, for the valence (green line), sea quark (blue), and gluon (red) PDFs, assuming 1.2% experimental systematic uncertainty but no model systematic uncertainty, and (inset) the corresponding ratios of the momentum fraction uncertainties, $\delta\langle x\rangle^{\mathrm{EIC}}/\delta\langle x\rangle$, for valence, sea, total quark and gluon PDFs [53], at a scale $Q^2 = 10$ GeV^2.

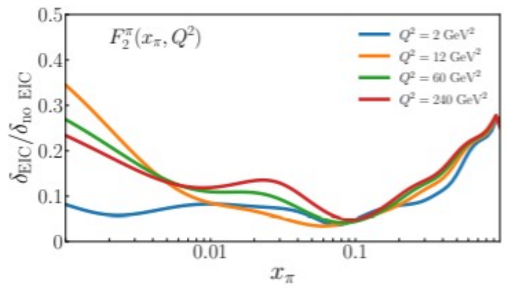

Figure 23: The ratio of the uncertainty of the F_2^π structure function from the global fit with and without including EIC projected data to the uncertainty of the F_2^π as a function of x_π for various Q^2 values.

ECCE - pion electromagnetic form factor

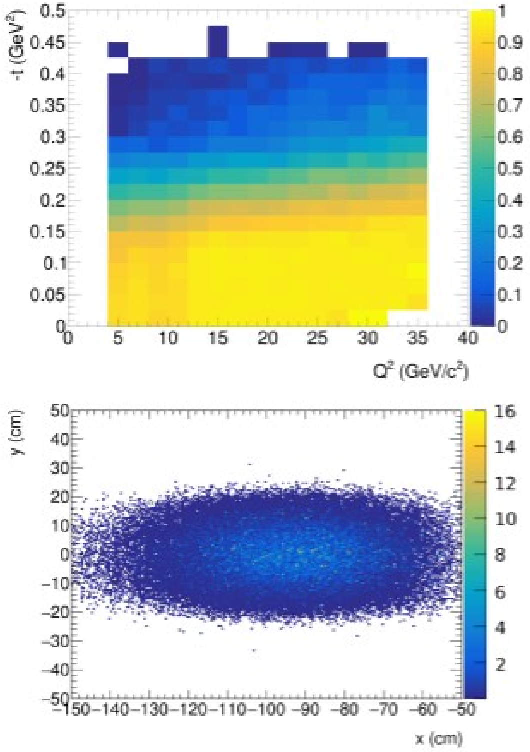

Figure 12: [Top] Detection efficiency for $e'\pi^+n$ triple coincidences in ECCE versus Q^2 and $-t$. [Bottom] Predicted distribution of neutron hits from the DEMP process in the ZDC.

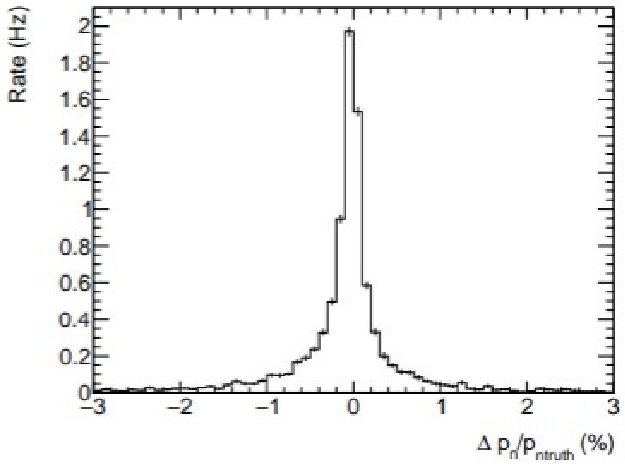

Figure 13: Deviation of the reconstructed neutron track momentum from the neutron "truth" track, expressed as a percentage, $\Delta p_n = (p_{ntrack} - p_{ntruth})/p_{ntruth}$ for $e'\pi^+n$ triple coincidence events.

ECCE - pion electromagnetic form factor

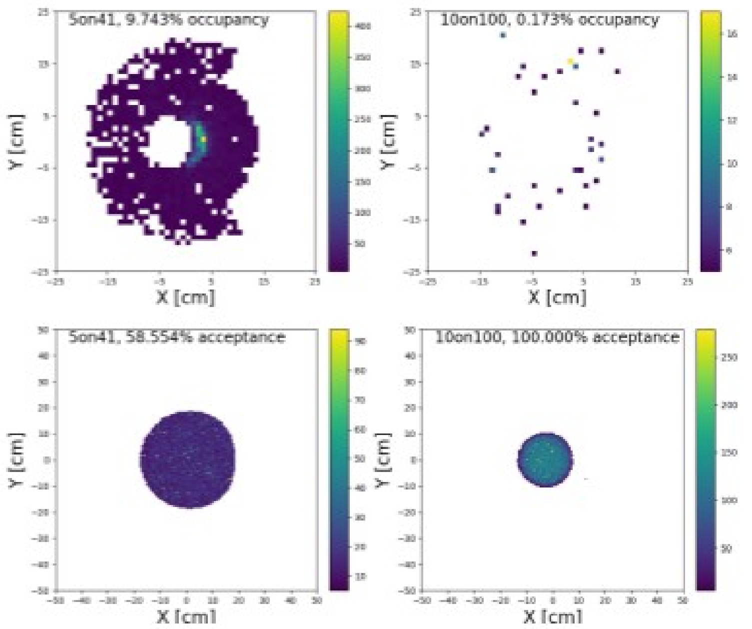

Figure 19: Top plots: B0 occupancy of the simulated leading neutron for $p(e, e'\pi^+n)$ meson structure study at 5×41 (left) and 10×100 (right). Bottom plots: ZDC acceptance of the simulated leading neutron for a range of energies 5x41 (left) and 10×100 (right).

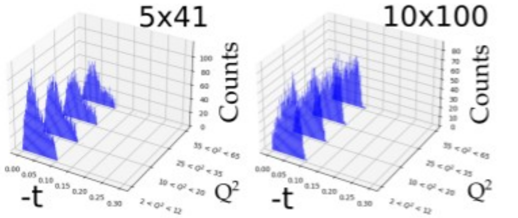

Figure 20: The $-t$ distributions of $p(e, e'\pi^+n)$ meson structure study at 5×41 (left) and 10×100 (right). There are four Q^2 bins presented (7, 15, 30, 60 GeV^2) of bin width ±5 GeV^2.

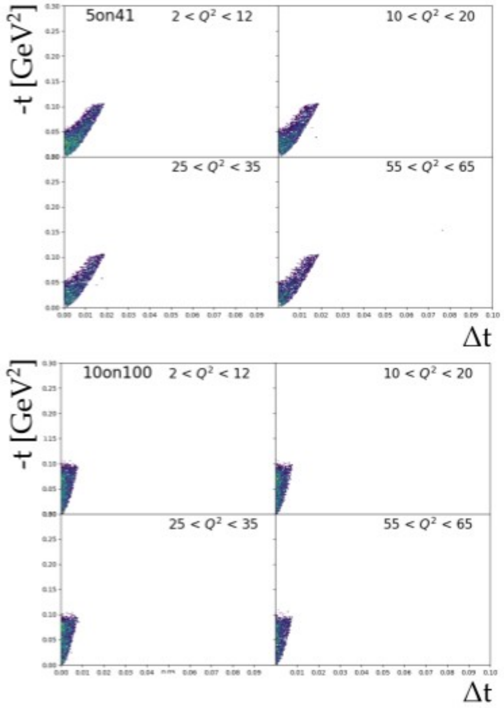

Figure 21: The deviation of generated $-t$ from the detected t_{truth} value for $p(e, e'\pi^+n)$ meson structure study, $\Delta t = t - t_{truth}$, for a range of energies (5×41, 10×100) at IP6. There are four Q^2 bins presented (7, 15, 30, 60 GeV^2) of bin width ±5 GeV^2. The lowest energy (5×41) sees a strong deviation. 5×41 is the same energy that sees the drop in ZDC acceptance.

ECCE - pion electromagnetic form factor

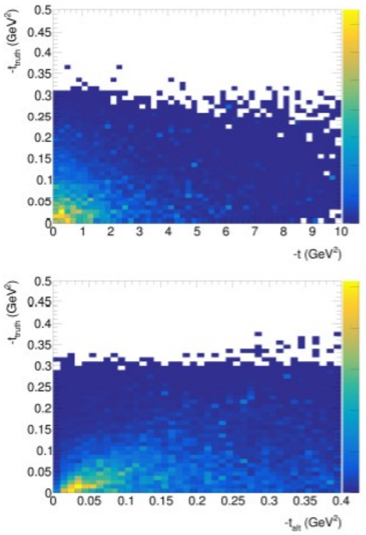

Figure 14: Reconstructed t versus true t for simulated $e'\pi^+n$ triple coincidence events with $15 < Q^2 < 20$ GeV^2, where t is reconstructed as $t = (p_e - p_{e'} - p_\pi)^2$ (top) and as $t_{alt} = (p_p - p_n)^2$ (bottom). p_n here is the reconstructed neutron track that combines the missing momentum with the ZDC position information. t reconstruction using the lepton and meson information alone shows little correlation with the true value (top), while the reconstruction from the charged tracks and the ZDC position information is more reliable. Note the vastly different horizontal scales of the two plots.

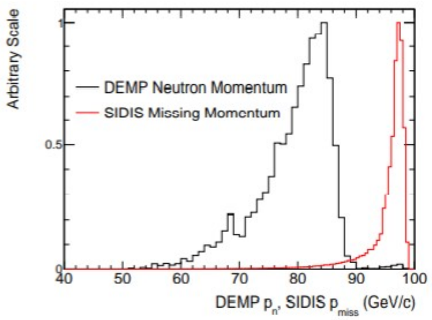

Figure 15: The reconstructed neutron track momentum for DEMP $e'\pi^+n$ triple coincidence events compared to $\vec{p}_{miss}$ for simulated SIDIS background events (y-axis scaled arbitrarily, $\vec{p}_{miss} = \vec{p}_e + \vec{p}_p - \vec{p}_{e'} - \vec{p}_{\pi^+}$). The SIDIS events can be cleanly separated from the DEMP events of interest. Note that both plots display events with $15 < Q^2 < 20$ GeV^2.

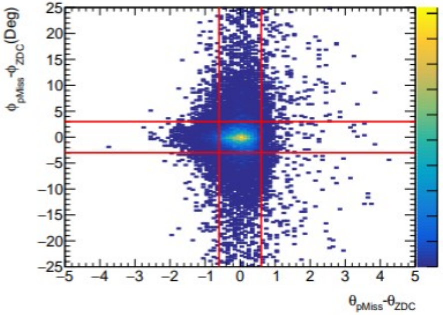

Figure 16: The difference between the reconstructed $(\theta_{pMiss}, \phi_{pMiss})$ and detected $(\theta_{ZDC}, \phi_{ZDC})$ simulated angles for the neutron in $e'\pi^+n$ triple coincidence events. The indicative cut range is shown by the area enclosed within the four red lines, $-0.6° < \theta_{pMiss} - \theta_{ZDC} < 0.6°$ and $-3° < \phi_{pMiss} - \phi_{ZDC} < 3°$.

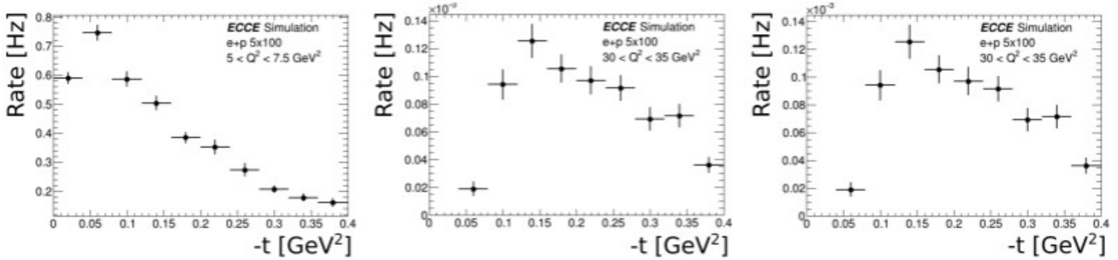

Figure 17: Predicted $e\pi^+n$ triple coincidence rates for different Q^2 bins after application of the p_{miss} and θ_n cuts described in the text. Each $-t$ bin is 0.04 GeV^2 wide. The luminosity assumed in these rate calculations: L= 10^{34} cm^{-2}s^{-1}.

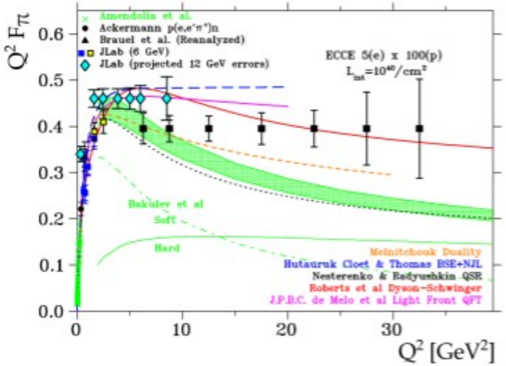

Figure 18: Existing data (blue, black, yellow, green) and projected uncertainties for future data on the pion form factor from JLab (cyan, red) and EIC (black), in comparison to a variety of hadronic structure models. The ECCE projections clearly cover a much larger Q^2 range than the JLab measurements, providing access to the emergent mass scale in QCD.

Figures in ATHENA/ECCE proposals

Kinematic coverage

- Either standard (Q2, x, t…) or channel specific

Detector oriented

- In which detector do the particles go, what coverage do we have
- Acceptance/efficiency of the detector setup
- Resolution figure to isolate this specific channel

Analysis exploration

- Observable resolution
- Background rates (pretty rare still)
- Different analysis techniques (or detector technologies)

The results plots

- Observable projections sometimes compared to existing data
- Global fit projections and phenomenology applied on pseudo data

Summary

We would like to start having an approved ePIC figures base

- It will be first implemented on the WG wiki pages
- We hope this review can inspire people doing the hard work of analysis and producing new figures
- The goal is not to constrain, but to encourage completeness and consistancy

And we can certainly be more consistant

- It will make easier to find figures in our documentation
- And easier to present our findings
  - **Internally to detector groups or reviews**
  - **Externally for conferences and publications**

Way Forward

Collaboration wide effort to make new figures

- Replace ATHENA/ECCE figures in talks
- Prepare the TDR figures
  - **And an associated physics paper**

Fits in our more general effort

- Create benchmarks to help the detector development process in the coming years
- Prepare for advanced analysis with pseudo-data
  - **Understand resolution, backgrounds…**